



HAL
open science

Mixed anion chemistry as a way to tune the electrochemical properties of vanadium oxyfluoride phosphates in alkali-ion batteries

Romain Wernert, Long Hoang Bao Nguyen, Dany Carlier, Laurence Croguennec

► To cite this version:

Romain Wernert, Long Hoang Bao Nguyen, Dany Carlier, Laurence Croguennec. Mixed anion chemistry as a way to tune the electrochemical properties of vanadium oxyfluoride phosphates in alkali-ion batteries. *Solid State Sciences*, 2023, 146, pp.107358. 10.1016/j.solidstatedsciences.2023.107358. hal-04285717

HAL Id: hal-04285717

<https://hal.science/hal-04285717>

Submitted on 14 Nov 2023

HAL is a multi-disciplinary open access archive for the deposit and dissemination of scientific research documents, whether they are published or not. The documents may come from teaching and research institutions in France or abroad, or from public or private research centers.

L'archive ouverte pluridisciplinaire **HAL**, est destinée au dépôt et à la diffusion de documents scientifiques de niveau recherche, publiés ou non, émanant des établissements d'enseignement et de recherche français ou étrangers, des laboratoires publics ou privés.

Mixed anion chemistry as a way to tune the electrochemical properties of vanadium oxyfluoride phosphates in alkali-ion batteries

Romain Wernert^{†‡Δ*}, Long H.B. Nguyen^{‡Δ}, Dany Carlier^{†Δ||}, Laurence Croguennec^{†Δ||*}

AUTHOR ADDRESS

† Univ. Bordeaux, CNRS, Bordeaux INP, ICMCB, UMR 5026, F-33600 Pessac, France

‡ ICGM, Université de Montpellier, CNRS, ENSCM, 34095 Montpellier, France

Δ RS2E, Réseau Français sur le Stockage Electrochimique de l'Energie, FR CNRS #3459, Amiens F-80039 Cedex 1, France

|| ALISTORE-ERI European Research Institute, FR CNRS 3104, F-80039 Amiens Cedex 1, France

* corresponding authors

KEYWORDS: vanadium oxyfluoride phosphate, mixed anion compounds, alkali-ion batteries,

ABSTRACT

Alkali vanadium fluoride phosphates such as *Tavorite* LiVPO_4F , $\text{Na}_3\text{V}_2(\text{PO}_4)_2\text{F}_3$ and KTP-type KVPO_4F are attractive materials for positive electrodes in rechargeable alkali-ion batteries. In such compounds, the presence of fluoride ions further increases the electrode's electrochemical potential compared to their phosphate counterparts such as $\text{Na}_3\text{V}_2(\text{PO}_4)_3$. Furthermore, the fluoride anions in these structures can be fully or partially substituted by oxide anions, leading to the formation of $\text{V}^{4+}=\text{O}$ vanadyl centres and a great number of mixed valence and mixed anion compositions. The oxygen substitution for fluorine has a considerable impact on the structural, electronic, and electrochemical properties of the resulting compounds. In this review, the similarities and peculiarities in the crystal structures, electronic structures, and electrochemical properties of the three analogous LiVPO_4F – LiVPO_4O , $\text{Na}_3\text{V}_2(\text{PO}_4)_2\text{F}_3$ – $\text{Na}_3\text{V}_2(\text{PO}_4)_2\text{FO}_2$, and KVPO_4F – KVPO_4O material families will be compared in detail. Such a comparison is expected to provide an insightful understanding on the factors governing the structure and properties of vanadium oxyfluoride phosphates.

INTRODUCTION

Vanadium phosphates are well known for their extensive crystal chemistry, owing to the variety of oxidation states and coordination polyhedra that vanadium can adopt.^{1,2} Among these compounds, V^{3+} and V^{4+} containing phosphates are of particular interest to be used as materials for positive electrode in rechargeable alkali-ion batteries. Despite the density and weight penalty of “large and heavy” PO_4 groups, phosphates remain attractive materials due to the stability of their frameworks (for long range cycling and safety issues) and the increased potential of a given $M^{n+}/M^{(n+1)+}$ redox couple compared to their oxide counterparts. The first vanadium phosphate possessing great electrochemical interests, $Na_3V_2(PO_4)_3$, was reported in 1978.³ This compound belongs to a structural family that is widely known as NASICON (Na Super Ionic CONductor). Following the booming of material research from the late 1990s, several vanadium fluoride phosphates, including $LiVPO_4F$, $NaVPO_4F$, $Na_3V_2(PO_4)_2F_3$, and $KVPO_4F$ were discovered; however, their applications as electrode materials for rechargeable alkali-ion batteries have just been reported in recent years.⁴⁻⁹ Comparing to their phosphate counterparts, the fluoride phosphate materials can offer a higher redox potential (**Figure 1**), which is beyond other different frameworks, mainly assigned to the inductive effective of F^- . For instance, a redox potential difference up to 0.5 V is observed in the case of $Na_3V_2(PO_4)_2F_3$ vs. $Na_3V_2(PO_4)_3$ (**Figure 1b**) which improves the energy density of the former by 26% compared to the latter. Such an increase in the redox potential can partially compensate for the capacity loss due to weight penalty of polyanion materials and hence allow vanadium phosphates to compete with layered oxide in terms of energy density.¹⁰

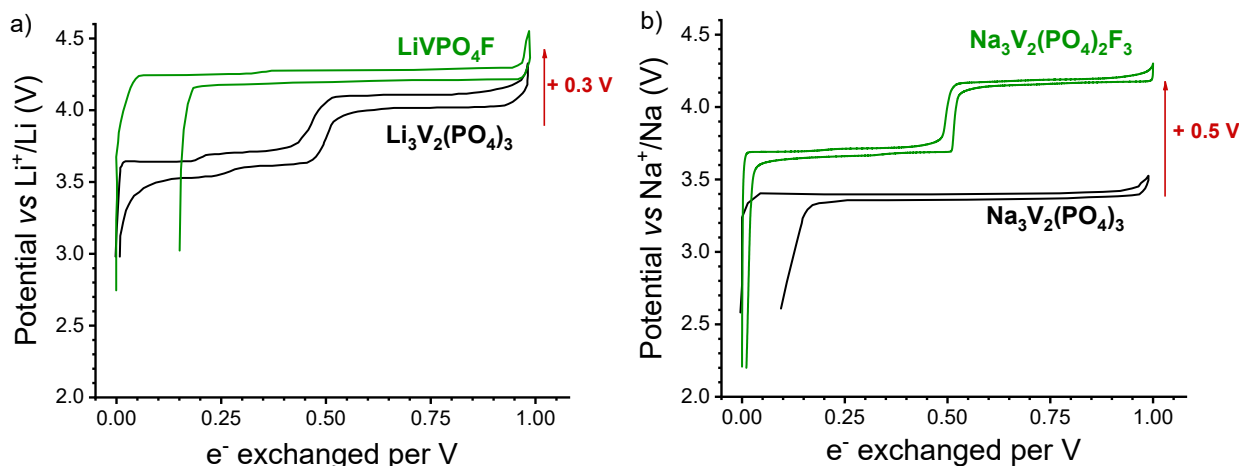


Figure 1: Comparison of the electrochemical curves of vanadium phosphates and vanadium fluoride phosphates positive electrode materials. a) Anti-NASICON $Li_3V_2(PO_4)_3$ and Tavorite $LiVPO_4F$ for Li-ion batteries. b) NASICON $Na_3V_2(PO_4)_3$ and $Na_3V_2(PO_4)_2F_3$ for Na-ion batteries.

In parallel to these trivalent vanadium fluoride phosphates, there exist homeotypic oxide phosphate compositions, *i.e.* $LiVPO_4O$, $Na_3V_2(PO_4)_2FO_2$, and $KVPO_4O$, which can also be used as positive electrode materials in batteries. In these oxide phosphates, F^- is replaced by O^{2-} , and all the vanadium ions present in the structure thus exist as V^{4+} to maintain the charge neutrality. Besides these fluoride and oxide phosphate end members, partially substituted oxyfluoride phosphates, such as $LiVPO_4F_{0.45}O_{0.55}$, were also reported in the literature.¹¹⁻¹³ Such a substitution can occur on all labile fluorine sites in the structure leading to an infinite number of compositions that differ in F/O content; nonetheless, well-controlled anionic stoichiometries can only be obtained from syntheses carried out under inert atmosphere. Even though the F/O substitution occurs only on the anionic framework, a significant impact might be observed on the atomic and electronic structure, alkali ion distribution, and thus structural, redox and diffusion mechanisms involved upon cycling, and more generally on the electrochemical properties in batteries. Throughout this review, three prominent vanadium fluoride phosphates, *i.e.* $LiVPO_4F$, $Na_3V_2(PO_4)_2F_3$, and $KVPO_4F$, will be discussed in detail to highlight the

impact of oxygen substitution for fluorine in each case and how it can be used to control the electrochemistry of vanadium fluoride phosphates. The Tavorite type NaVPO_4F derived materials obtained by a high temperature solid state synthesis were shown earlier to provide limited interest as positive electrode materials due to the low mobility of Na^+ ions and will hence be excluded from this work.¹⁴

CRYSTAL STRUCTURES

LiVPO_4F , $\text{Na}_3\text{V}_2(\text{PO}_4)_2\text{F}_3$ and KVPO_4F are undoubtedly the most well-studied vanadium fluoride phosphates. These compounds can be obtained by a direct synthesis between the alkali fluoride AF ($\text{A} = \text{Li}, \text{Na}, \text{K}$) and vanadium phosphate, VPO_4 , in the right stoichiometry under inert atmosphere. These compounds crystallise in three different structural types as shown in **Figure 2**. Despite the difference in their long-range structures, they are constructed based on the same structural building units, *i.e.* VO_4F_2 octahedra and PO_4 tetrahedra. The stoichiometry (AVPO_4F or $\text{A}_{1.5}\text{VPO}_4\text{F}_{1.5}$) and the radius of the alkali ion (0.76, 1.02 and 1.38 Å for Li^+ , Na^+ and K^+ respectively) are indeed the key factors determining the thermodynamic stability of the phase formed during the synthesis.

LiVPO_4F belongs to the triclinic ($P\bar{1}$) Tavorite structural type and shows a zigzag quasi-1D diffusion pathway for Li^+ ions.^{5,6} The fluorine atoms in the VO_4F_2 unit are localized in the apical positions and these *trans*- VO_4F_2 units are connected via F-corner sharing to form infinite chains of $[\text{F}-\text{VO}_4-\text{F}]_\infty$ running parallel to each other and connected by PO_4 tetrahedra (**Figure 2**). The crystal structure of $\text{Na}_3\text{V}_2(\text{PO}_4)_2\text{F}_3$ is often falsely claimed as being NASICON, although they share no crystal features in common: the lantern unit typical of NASICON structure $(\text{VO}_6)_2(\text{PO}_4)_3$ are not observed in $\text{Na}_3\text{V}_2(\text{PO}_4)_2\text{F}_3$.¹⁵⁻¹⁷ The crystal structure of $\text{Na}_3\text{V}_2(\text{PO}_4)_2\text{F}_3$ (*Amam*) is also built up from *trans*- VO_4F_2 units; however, the vanadium unit extension is only limited to $\text{FO}_4\text{V}-\text{F}-\text{VO}_4\text{F}$ bioctahedra aligned along the *c* direction and maintained together by PO_4 groups in the (*a*, *b*) plane (**Figure 2**). $\text{Na}_3\text{V}_2(\text{PO}_4)_2\text{F}_3$ shows a quasi-2D diffusion pathway for Na^+ ions.^{7,18} Finally, KVPO_4F crystallises in the non-centrosymmetric KTiOPO_4 (KTP) type structure (*Pna2*₁) and shows a quasi-1D diffusion pathway for diffusion of K^+ ions.^{8,9} Although the stoichiometry is analogous to Tavorite type LiVPO_4F , the structure is very different and should not be confused. The KTP structure features also chains of F-corner sharing VO_4F_2 octahedra; however, the fluorine positions on two adjacent VO_4F_2 units are alternating between *cis* and *trans* configurations, and the connection between these $[\text{VO}_4\text{F}_2]_\infty$ chains is also ensured by PO_4 groups (**Figure 2**). Despite differences in the three crystalline structures, the V^{3+} local environment is in all cases quasi-symmetric with all the $\text{V}^{3+}-\text{X}$ bonds length ($\text{X} = \text{F}$ or O) almost identical (~ 1.98 Å) regardless the nature of the ligand.

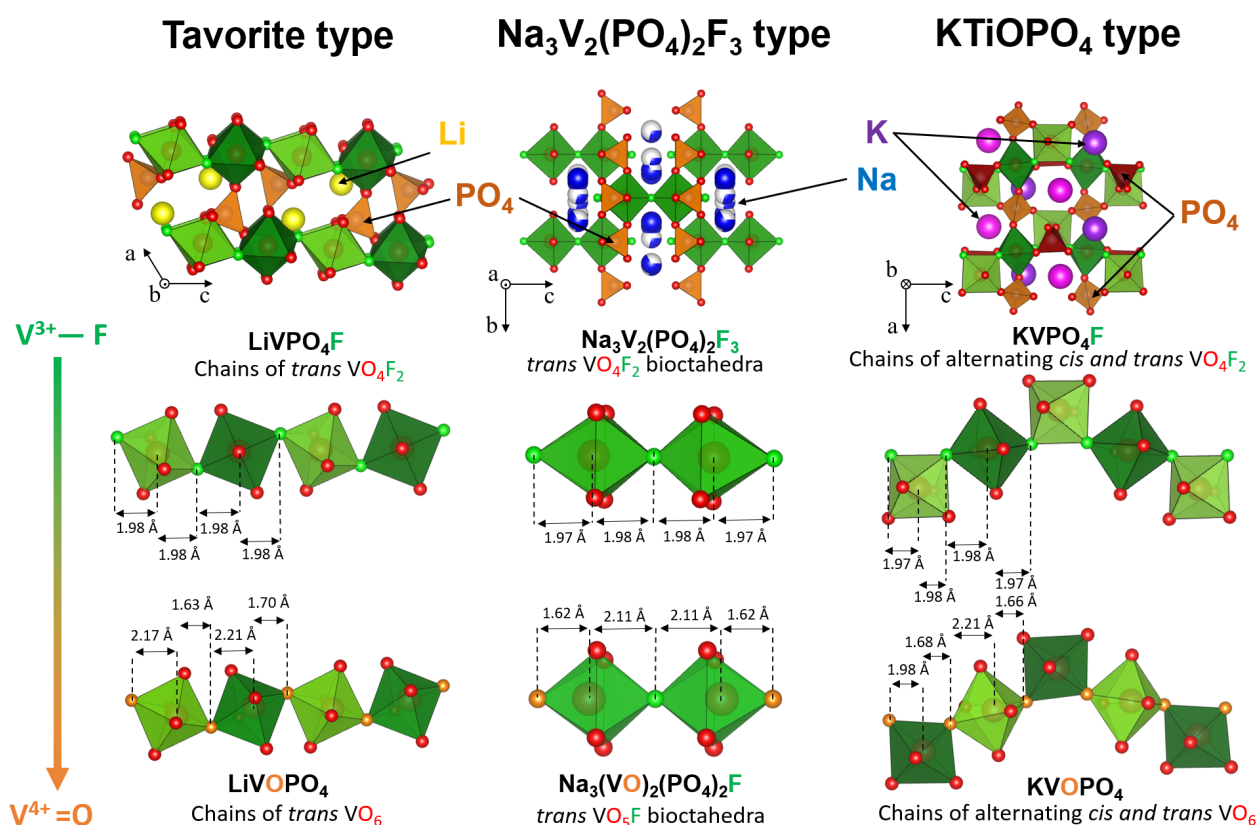


Figure 2: Comparison of the crystal structures of Tavorite-type LiVPO₄(F,O), Na₃V₂(PO₄)₂F(F,O)₂ and KTP-type KVPO₄(F,O). The topology and the connectivity of the vanadium polyhedra are shown below each crystal structure.

The corresponding vanadium oxide phosphates LiVPO₄O, Na₃V₂(PO₄)₂FO₂, and KVPO₄O can be obtained from the syntheses using V³⁺-containing precursor together with a stoichiometric amount of oxidant, *e.g.* VOPO₄, or combining V⁵⁺-containing precursor with an appropriate reduction. The structures of these V⁴⁺ oxide phosphates are closely related to their fluoride phosphate counterparts with all (or some) of the fluorine positions now occupied by oxygen. LiVPO₄O also crystallises in the Tavorite structure; however, along the [O–VO₄–O]_∞ chains the V–O distances alternate between a short (~ 1.67(3) Å) and a long (~ 2.19(2) Å) one. Similarly, in KVPO₄F all the fluorine sites (with *cis* and *trans* configurations) can be replaced by oxygen to obtain KVPO₄O. An alternating between short (~ 1.66 Å) and long (~ 2.11 Å) V–O bonds is only observed on the *trans* sites. On the *cis* sites, a shortened V–O bond (~ 1.66 Å) is evident, but no elongation is detected (**Figure 2**): all the other five V–O distances are similar (~ 2.01 Å). In Na₃V₂(PO₄)₂F₃, there exist two different fluorine sites in the FO₄V–F–VO₄F bioctahedron; however, only the one corresponding to the outer apical site can be replaced by oxygen to generate the homologue Na₃V₂(PO₄)₂FO₂. In the O–VO₄–F unit the V–O bond is shortened to ~ 1.62 Å while the opposite V–F bond is elongated to ~ 2.11 Å, in comparison to ~ 1.98 Å in Na₃V₂(PO₄)₂F₃.

When moving from fluoride phosphates to oxide phosphates, all V³⁺ in the structure are oxidised into V⁴⁺ to maintain the charge neutrality. Furthermore, the V⁴⁺ is shifted out of the centre of the VO₆ octahedron that lowers the local symmetry of the vanadium site from “quasi”-O_h to C_{4v}.¹⁹ This local structural distortion leads to two important consequences: (i) the *t*_{2g} (*d*_{xy}, *d*_{xz}, and *d*_{yz}) levels of V⁴⁺ are split into two groups *e* (*d*_{xz}, *d*_{yz}) and *b*₂ (*d*_{xy}), and (ii) the π-bonding interaction that stabilises the occupied nonbonding O 2*p* states is enhanced due to the shorter distance between the vanadium center and the apical oxygen. The distorted V⁴⁺O₆ octahedron is more energetically favourable than the non-distorted one thanks to the energetic stabilisation of (i) occupied *d*_{xy} states of V⁴⁺ and (ii) occupied nonbonding O 2*p* states. The short V–O bond (~ 1.66 Å) detected in all vanadium oxide phosphates involves a strong σ and a strong π interaction. This chemical bond is widely known as

“vanadyl” bond or V=O. As the vanadyl bond becomes highly covalent, the V–O bond opposite to it becomes highly ionic with an elongated distance up to $\sim 2.19(2)$ Å. This antagonist behaviour is observed in LiVPO_4O , $\text{Na}_3\text{V}_2(\text{PO}_4)_2\text{FO}_2$ and for the *trans*- VO_6 site in KVPO_4O . For the *cis*- VO_6 site in KVPO_4O , the O ions of the V–O bond opposite to V=O is engaged in a P–O bond, which prevents a full elongation.

A particular feature of these vanadium fluoride/oxide phosphates is the existence of the mixed oxyfluoride phosphate compositions, *i.e.* $\text{LiVPO}_4\text{F}_{1-y}\text{O}_y$ ($0 < y < 1$), $\text{Na}_3\text{V}_2(\text{PO}_4)_2\text{F}_{3-y}\text{O}_y$ ($0 < y < 2$) and $\text{KVPO}_4\text{F}_{1-y}\text{O}_y$ ($0 < y < 1$). Depending on the oxidation state of vanadium in the precursors, these compositions can be obtained by introducing a certain amount of oxidant or reductant during the synthesis process. Nonetheless, the main challenge in the synthesis of these compounds is the accurate control of the F/O content, which greatly depends on the nature of the precursors and the reaction conditions. Using diffraction techniques, $\text{Na}_3\text{V}_2(\text{PO}_4)_2\text{F}_{3-y}\text{O}_y$ ($0 \leq y \leq 2$) and $\text{KVPO}_4\text{F}_{1-y}\text{O}_y$ ($0 \leq y \leq 1$) are determined to form a complete solid solution with a linear evolution in the cell parameters (*a*, *b*, and *c*) over the full range of F/O content, implying that F and O are randomly distributed on the mixed anionic sites. On the other hand, the cell parameters of Tavorite $\text{LiVPO}_4\text{F}_{1-y}\text{O}_y$ ($0 \leq y \leq 1$) deviate significantly from the Vegard’s law (**Figure 3a**). The reason behind this deviation is the segregation of VO_6 units upon oxygenation, which could be detected using X-ray diffraction but fully explained by solid state nuclear magnetic resonance (ss-NMR) spectroscopy as illustrated in **Figure 3b**.

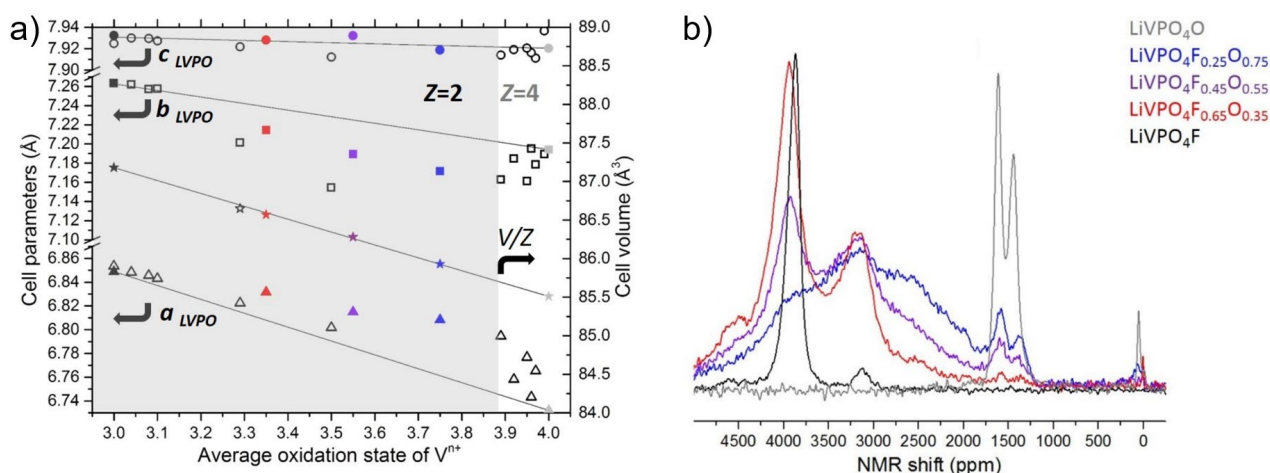


Figure 3: a) Evolution of cell parameters (*a*: triangles, *b*: squares and *c*: circles) and *V/Z* of $\text{LiVPO}_4\text{F}_{1-y}\text{O}_y$.²⁰ b) ^{31}P MAS NMR spectra of $\text{LiVPO}_4\text{F}_{1-y}\text{O}_y$ phases, adapted from ref²¹ with permission from John Wiley and sons.

As the oxygen substitution for fluorine can occur on the full range of compositions, an accurate determination of the F/O content is essential to establish the relationship between the composition and the physicochemical properties of the materials, as well as to be able to propose a synthesis process with the ability to finely tune the composition. Due to similarity in their X-ray and neutrons scattering factors, a direct probing of F^- and O^{2-} by diffraction techniques is not possible. As the Vegard’s law is observed for $\text{Na}_3\text{V}_2(\text{PO}_4)_2\text{F}_{3-y}\text{O}_y$ ($0 \leq y \leq 2$) and $\text{KVPO}_4\text{F}_{1-y}\text{O}_y$ ($0 \leq y \leq 1$), the cell parameters of references, such as the end members, can be used to establish calibration curves and determine the *y* value in a new composition. Energy dispersive X-ray spectroscopy (EDX) can also be used to obtain an approximative value of the F/O content; however, it should be kept in mind that this technique is not accurately quantitative for light elements and a suitable reference is usually required.²² Electrochemical methods such as F^- ion-selective electrode can also be used provided a considerable amount of powder is available.^{23–25}

LOCAL STRUCTURE EVOLUTION AND SPECTROSCOPIC CHARACTERISATION

As discussed above, oxygen substitution for fluorine in these structures induces the formation of vanadyl bonds ($V^{4+}=O$). The stretching modes of these vanadyl bonds are active on both infrared (IR) and Raman spectroscopies, with an intense signal usually observed at $\sim 900\text{ cm}^{-1}$.²⁶ In IR spectroscopy, this vibrational band slightly overlaps with the bands of P–O stretching modes in PO_4 group; however, the activity of P–O stretching bands is greatly reduced in Raman spectroscopy, and thus the visibility of $V=O$ band is enhanced significantly.²⁷ Either IR or Raman spectroscopy is employed, the intensity of $V=O$ stretching band increases gradually with the O-substitution rate in all $LiVPO_4F_{1-y}O_y$, $Na_3V_2(PO_4)_2F_{3-y}O_y$ and $KVPO_4F_{1-y}O_y$ (as highlighted in **Figure 4a** for $Na_3V_2(PO_4)_2F_{3-y}O_y$), which is an effective and rapid probe for the existence of O-substitution in the structure.

When O-substitution occurs, V^{3+} is simultaneously oxidised into V^{4+} for charge compensation. The extent of the F/O substitution can thus be deduced from the V^{3+}/V^{4+} ratio. Vanadium *K*-edge X-ray absorption spectroscopy (XAS) is a technique that can directly access the local environment and oxidation state of vanadium species in the structure. Every X-ray absorption near edge structure (XANES) spectrum can be divided into the pre-edge and edge regions. The signal in the pre-edge region is generated from the transitions of vanadium $1s$ core states to its empty $3d$ states, which are only allowed in non-centrosymmetric environments, *i.e.* V^{4+} involved in the vanadyl bond. The intensity of this signal is directly proportional to the amount of substituted O in the structure (as highlighted in **Figure 4b** for $KVPO_4F_{1-y}O_y$ as well as in **Figure 4c** where each oxygen rich end-member displays a very intense pre-edge), which can be used as qualitative probe for the presence of vanadyl bonds, as in the case of IR or Raman spectroscopy. The edge signal originates from the allowed $1s \rightarrow 4p$ transitions, and its position is closely related to the oxidation state of the vanadium species. The edge position will shift to higher energies in higher oxidation states, which will help to determine the average oxidation state of vanadium, and thus the V^{3+}/V^{4+} and F/O ratios for a given composition. Nonetheless, the edge energy is also dependent on the vanadium's surrounding environment, and in the best scenario, some standards of similar crystal structure are required to establish a calibration curve (**Figure 4b**). This technique can be precise to *c.a.* 5% but is not relevant for very small substitution rates.

These material families contain several easily accessible NMR active nuclei (${}^6/7Li$, ${}^{19}F$, ${}^{23}Na$, ${}^{31}P$, and ${}^{51}V$), which can be investigated to provide insightful information on the local environments in the structure.^{13,21,24,28–31} Among them, ${}^{31}P$ ss-NMR is widely studied and can reveal similarities and differences between these crystal structures at the atomic scale. The phosphorus atoms in these structures are tetrahedrally coordinated with four neighbouring vanadium octahedra giving rise to the $P(OV)_4$ sub-units. As all the compounds in these three material families contain paramagnetic ions, *i.e.* V^{3+} and/or V^{4+} , the Fermi contact would be the dominant interaction leading to highly shifted ${}^{31}P$ NMR resonances. Experimental work coupled with theoretical modelling have shown that the magnitude of ${}^{31}P$ NMR shifts in these three systems depends significantly on the distribution of V^{3+}/V^{4+} in the $P(OV)_4$ sub-unit, and the spin transfer pathway between vanadium ions and the phosphorus nucleus. Other parameters, such as torsion angle, V–P distance, V/P–O bond length, thus also play a role as they directly impact the spin transfer pathway. In $LiVPO_4F_{1-y}O_y$ and $KVPO_4F_{1-y}O_y$, well-defined ${}^{31}P$ ss-NMR resonances corresponding to $P(OV^{3+})_4$ and $P(OV^{4+})_4$ are observed for V^{3+} and V^{4+} -containing end members. The ${}^{31}P$ resonances in $LiVPO_4F$ and $KVPO_4F$ are greatly shifted compared to their oxide phosphate counterparts as V^{3+} possesses two unpaired electrons versus only one for V^{4+} and thus the Fermi contact in $P(OV^{3+})_4$ is stronger than $P(OV^{4+})_4$, as quantified in **Table 1**.^{13,21} When the O-substitution occurs, new resonances corresponding to $P(OV^{3+})_3(OV^{4+})$, $P(OV^{3+})_2(OV^{4+})_2$, and $P(OV^{3+})(OV^{4+})_3$ local environments emerge. Nevertheless, these new resonances are rather broad leading to significant overlapping and preventing a clear deconvolution of the signals. The same scenario is observed for $Na_3V_2(PO_4)_2F_{3-y}O_y$; however, all the ${}^{23}Na$ and ${}^{31}P$ NMR resonances in this system are well separated, and thus the relative ratio between all local environments can be deduced when the acquisition is performed in quantitative conditions.²¹ Despite still difficult sometimes to be interpreted, ${}^{19}F$ ss-NMR is interesting to be studied.^{21,32} In Tavorite structure, fluorine nuclei are surrounded by two vanadium ions in the $[F-VO_4-F]_{\infty}$ chains. Theoretically, when substituted by oxygen for fluorine, a statistical distribution of O/F in oxyfluoride $LiVPO_4F_{1-y}O_y$ ($0 < y < 1$) should lead to two different fluorine local environments, *i.e.* $V^{3+}-F-V^{3+}$ and $V^{3+}-F-V^{4+}$; in fact, only the $V^{3+}-F-V^{3+}$ environment

is experimentally detected showing that substituted oxygens in Tavorite structure are not randomly distributed, but segregated into O-rich domains next to F-rich domains.^{21,33}

Table 1: ^{31}P MAS NMR Fermi contact shifts for end member compounds of the $\text{LiVPO}_4\text{F}_{1-y}\text{O}_y$, $\text{Na}_3\text{V}_2(\text{PO}_4)_2\text{F}_{3-y}\text{O}_y$ and $\text{KVPO}_4\text{F}_{1-y}\text{O}_y$ compounds.

Site	$\text{LiVPO}_4\text{F}_{1-y}\text{O}_y$		$\text{Na}_3\text{V}_2(\text{PO}_4)_2\text{F}_{3-y}\text{O}_y$	$\text{KVPO}_4\text{F}_{1-y}\text{O}_y$	
	P(1)	P(2)	P(1)	P(1)	P(2)
$\text{V}^{3+}\text{-F}$	4000		6000	5800	4400
$\text{V}^{4+}\text{=O}$	1600	1400	0	2000	1000

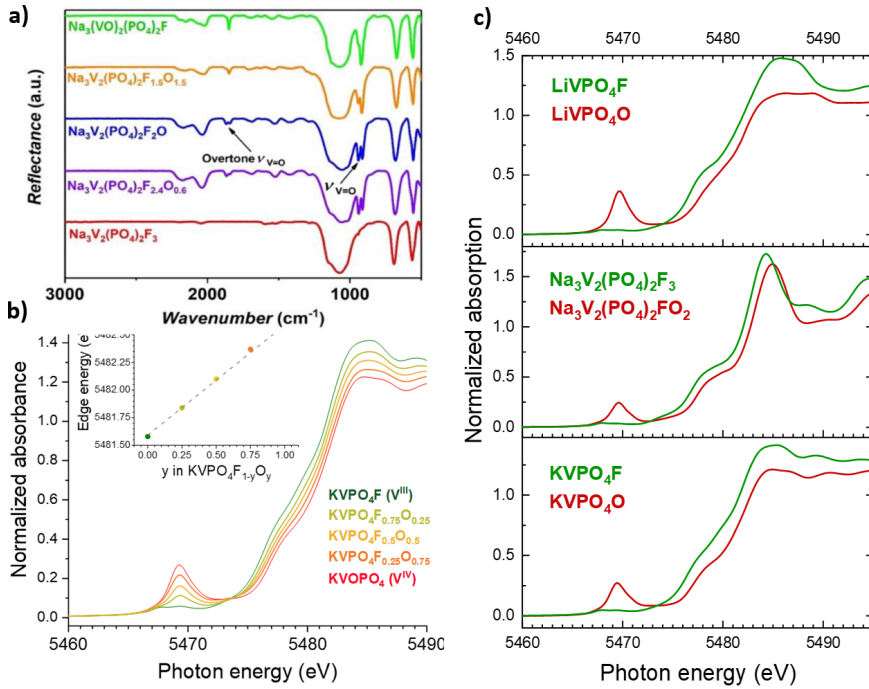


Figure 4: a) FTIR spectra of $\text{Na}_3\text{V}_2(\text{PO}_4)_2\text{F}_{3-y}\text{O}_y$, b) V K-edge XAS of $\text{KVPO}_4\text{F}_{1-y}\text{O}_y$, adapted with permission from ref¹³ Copyright 2022 American Chemical Society, and c) V K-edge XAS of oxygen-rich and fluorine-rich end-members in $\text{LiVPO}_4\text{F}_{1-y}\text{O}_y$, $\text{Na}_3\text{V}_2(\text{PO}_4)_2\text{F}_{3-y}\text{O}_y$ and $\text{KVPO}_4\text{F}_{1-y}\text{O}_y$.

A detailed comparison of these three systems has shown that the O-substitution has a great impact on the average and local structures of the materials. Regardless of the nature of the system, the O-substitution leads to the formation of distorted vanadium sites and highly covalent vanadyl bonds. The presence of these vanadyl bonds can be easily evaluated using vibrational spectroscopy or the pre-edge signature on the V K-edge XANES spectra. Despite these similarities, those systems exhibit subtle differences in the F/O distribution and the local environments of other atoms. In $\text{LiVPO}_4\text{F}_{1-y}\text{O}_y$, the O/F atoms are not randomly distributed along the chains, but segregated at the local scale. This behavior results in a deviation from the Vegard's law when examining the cell parameters, and thus V K-edge XAS is more informative to determine the F/O content in the structure. For $\text{Na}_3\text{V}_2(\text{PO}_4)_2\text{F}_{3-y}\text{O}_y$ and $\text{KVPO}_4\text{F}_{1-y}\text{O}_y$, the Vegard's law is obeyed, and thus the use of diffraction techniques together with some standard samples would suffice to obtain reliable F/O content. Finally, each member in the $\text{Na}_3\text{V}_2(\text{PO}_4)_2\text{F}_{3-y}\text{O}_y$ family gives rise to distinct and well-defined signatures on ^{23}Na and ^{31}P ss-NMR that can be easily deconvoluted and used in the compositional determination. With the accurate determination of the chemical formula, those materials can now be tested in different applications to understand the impact of O-substitution on the properties of the materials. In the context of this review, only the electrochemical properties will be further discussed.

ELECTROCHEMICAL PROPERTIES

All the compositions in the three systems are electroactive and can be used as positive electrode materials for alkali ion rechargeable batteries. Even though the host structures are quite versatile and one material might be used in different battery technologies, the following discussions will be limited in the case where the mobile ion is the same as in the host structure.

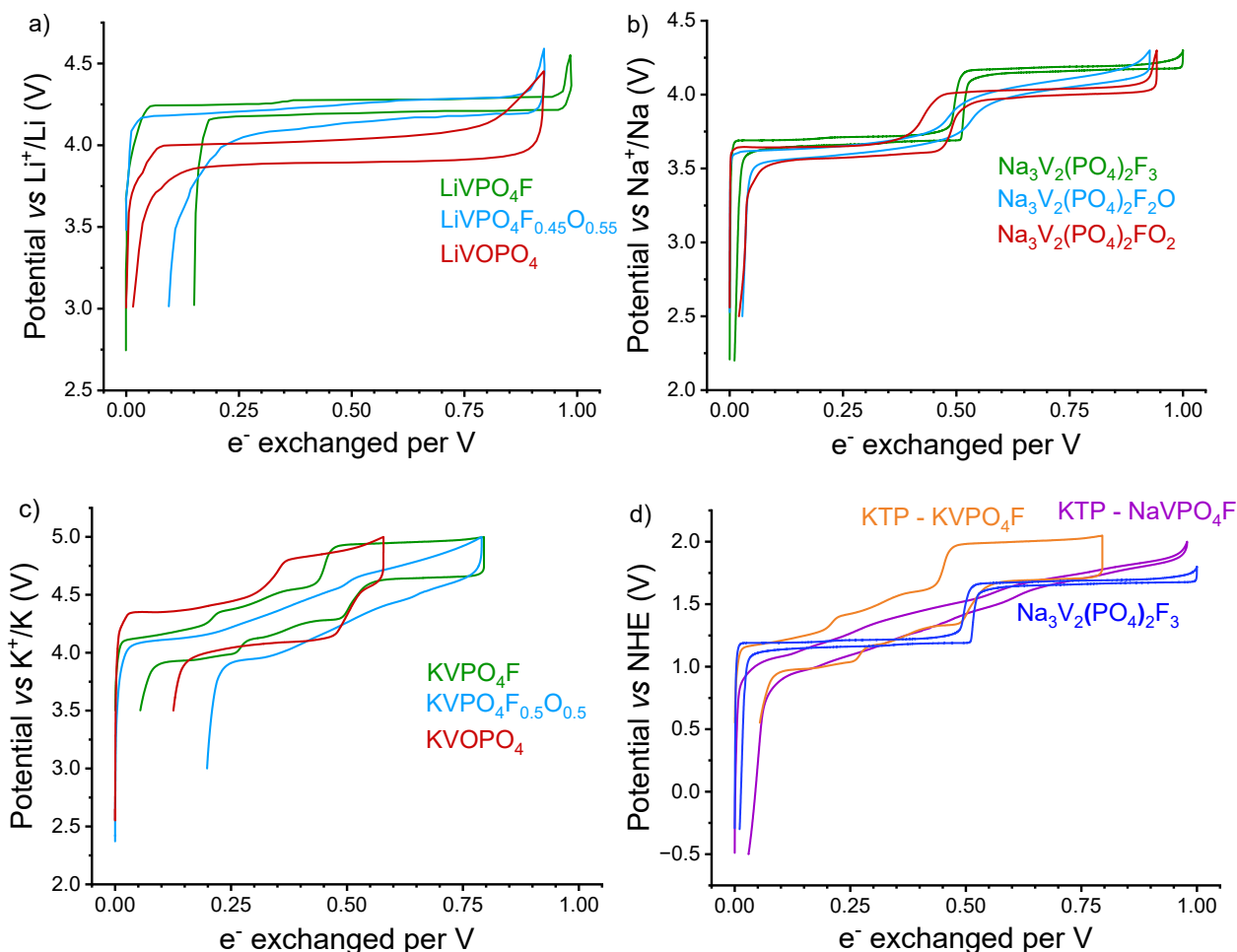


Figure 5: a-c) Comparison of the galvanostatic electrochemical curves of LiVPO₄(F,O), Na₃V₂(PO₄)₂F(F,O)₂ and KVPO₄(F,O) cycled versus their respective alkali metal counter electrode at a C/20 current rate. d) Comparison of the electrochemical curves of KVPO₄F vs. K metal, NaVPO₄F obtained by ion exchange from KTP vs NH₄VPO₄F vs Na metal,³⁴ and Na₃V₂(PO₄)₂F₃ vs Na metal reference vs NHE.

All members in the LiVPO₄F_{1-y}O_y series can allow the reversible extraction and re-insertion of one Li⁺ per formula unit in the voltage range of 3.0 – 4.5 V vs Li⁺/Li (**Figure 5a**). The presence of the flat voltage plateau implies that the delithiation process would occur through biphasic reaction for all compositions. However, meticulous *operando* diffraction measurements disclosed complicated electrode reaction mechanisms: (i) two successive biphasic reactions together with the formation of Li_{2/3}VPO₄F as intermediate phase is detected in charge for LiVPO₄F and an asymmetric reaction in discharge with a single biphasic reaction,³⁵ (ii) a single reversible biphasic reaction is observed for LiVPO₄O, and (iii) successively and reversibly, one monophasic and two biphasic reactions for all partially O-substituted LiVPO₄F_{1-y}O_y. The complexity in the reaction mechanism of partially substituted phases is the existence of the different F- and O-rich domains, inducing local inhomogeneous delithiation at the atomic scale. In LiVPO₄F, all the redox centres are V³⁺-F and they are oxidised into V⁴⁺-F during delithiation. When O-substitution occurs, V⁴⁺=O centres are generated, which are

further oxidised into $V^{5+}=O$ upon delithiation. In $LiVPO_4F_{1-y}O_y$, $V^{4+}=O$ is oxidised at a lower potential than $V^{3+}-F$, which can be explained by the “reverse inductive effect” due to the difference in the covalent $V^{4+}=O$ bonds compared to ionic $V^{3+}-F$. Consequently, the redox potential of the material will shift to lower value when the O-content increases, ultimately reaching a difference of -0.3 V for $LiVPO_4O$ compared to $LiVPO_4F$.

A similar situation is also observed for $Na_3V_2(PO_4)_2F_{3-y}O_y$ (**Figure 5b**) with the exchange of one electron per vanadium redox centre upon charge and discharge of the battery. For the two end members, the presence of two main plateaus indicates biphasic reactions upon charge and discharge. *Operando* diffraction/spectroscopy measurements coupled with theoretical calculations reveal that the voltage jump at $Na_2V_2(PO_4)_2F_3$ and $Na_2V_2(PO_4)_2FO_2$ corresponds to the V^{3+}/V^{4+} charge ordering on the bioctahedral units in the structure while several Na^+ -vacancy orderings are detected for other key compositions, but with much smaller voltage jumps. The voltage jump due to charge ordering on the octahedra is still obvious in partially O-substituted phases.^{18,19,24,36} Furthermore, the $V^{4+}=O$ redox centres in $Na_3V_2(PO_4)_2F_{3-y}O_y$ are oxidised at a potential that is slightly lower than that of $V^{3+}-F$ (down by 0.1 V for the fully oxygenated end-member). Increasing the substitution rate will lower the redox potential, but it is not as important as in $LiVPO_4F_{1-y}O_y$. Due to a small difference in their activation potential, $V^{4+}=O$ and $V^{3+}-F$ are oxidised simultaneously in partially O-substituted compositions.

In $KVPO_4F_{1-y}O_y$ (**Figure 5c**), the number of exchanged electrons is slightly less than one per vanadium ion in batteries versus K metal. However, the redox potential in those materials is so high that an upper cut-off voltage of 5.0 V vs K^+/K is required, and the limited number of electrons exchanged is a limitation of the employed electrolyte.³⁷ The voltage–composition curve of $KVPO_4F$ is dominated by four different K^+ -vacancy orderings.²³ Furthermore, the voltage jump at $K_{0.5}VPO_4F$ is assigned to the change in the vanadium site that participates in the redox reactions: whereas $LiVPO_4F$ and $Na_3V_2(PO_4)_2F_3$ only possess *trans* VO_4F_2 sites, the KTP structure features a *cis* and a *trans* VO_4F_2 site and it was demonstrated that the *cis*- VO_4F_2 sites are preferentially oxidised when K^+ is deintercalated up to the composition $K_{0.5}VPO_4F$, and that further K^+ removal leads to the oxidation of *trans*- VO_4F_2 .³⁸ Contrary to previous observations made for the two other systems, the $V^{4+}=O$ redox centres in partially O-substituted $KVPO_4F_{1-y}O_y$ are oxidised after $V^{3+}-F$. Furthermore, the redox potential of $KVPO_4O$ is even higher than that of $KVPO_4F$.

In all three systems, the substitution of O for fluorine has a great impact on the redox mechanism involved upon cycling. In $LiVPO_4F_{1-y}O_y$ and $Na_3V_2(PO_4)_2F_{3-y}O_y$, O-substitution results in the formation of $V^{4+}=O$ redox centres which oxidised at (slightly) lower potentials, shifting down the whole redox potential of the material; however, reverse behaviour is observed for $KVPO_4F_{1-y}O_y$. Furthermore, in a recent study, $NaVPO_4F$, synthesised through an ion exchange from KTP type NH_4VPO_4F , has revealed an electrochemical signature (*i.e.* number of exchanged electrons per vanadium and voltage-composition curve) completely different from $KVPO_4F$ (**Figure 5d**).³⁴ Indeed, depending on the ionic radii of the alkali ion, different alkali-vacancies orderings are stabilized during the alkali deintercalation in order to mitigate the electrostatic repulsions between them: it appears that the bigger the alkali ion is, the more phase transitions are observed upon charge and discharge, as also demonstrated for A_xMO_2 layered oxides. Furthermore, it can be seen on **Figure 6** that the average electrochemical potential of all the fluoride rich composition is nearly identical (1.4 V vs NHE) whereas there is a large variation for the three vanadyl phosphates. It is yet unclear whether this is really due to a size effect of the A^+ cations, but a sensible explanation would be that the topology of the shortened $V=O$ and elongated $V-O$ bonds matters a lot (**Figure 2**) as it has a huge influence on the $V-V$ distances and the Coulombic interaction that results.

Playing with the anionic chemistry is one of the routes explored to develop high voltage electrode materials for high energy density alkali ion batteries. As discussed here, this substitution leads to the formation of highly covalent vanadyl type $V=O$ bonds and it appears that the electrode reactions are highly reversible if V^{5+} ions (when formed) are localized in these sites that can be distorted thanks to the presence of vanadyl type $V=O$ bonds. All the polyanionic materials mentioned here are thus promising as alternative high energy density materials for Li, Na and K-ion batteries, *i.e.* with $LiVPO_4(F,O)$, $Na_3V_2(PO_4)_2F(F,O)_2$ and $KVPO_4(F,O)$ respectively. It is interesting to mention that cationic substitution has also been widely explored in the last few years in order to increase the energy density delivered for instance by the NASICON type material $Na_3V_2(PO_4)_3$.

Iron and manganese substitutions allowed the formation of sodium rich compositions, *i.e.* $\text{Na}_4\text{FeV}(\text{PO}_4)_3$ and $\text{Na}_4\text{MnV}(\text{PO}_4)_3$.^{39–43} The exchange of more than one electron per transition metal ions was demonstrated, but strong irreversibility was observed as soon as the oxidation of V^{3+} to V^{5+} was activated. Indeed, in these cases, all oxygen atoms in VO_6 units are covalently bonded to PO_4 groups, and thus VO_6 cannot be distorted to accommodate V^{5+} formation, leading to the migration of vanadium to reduce the energy of the system.³⁹

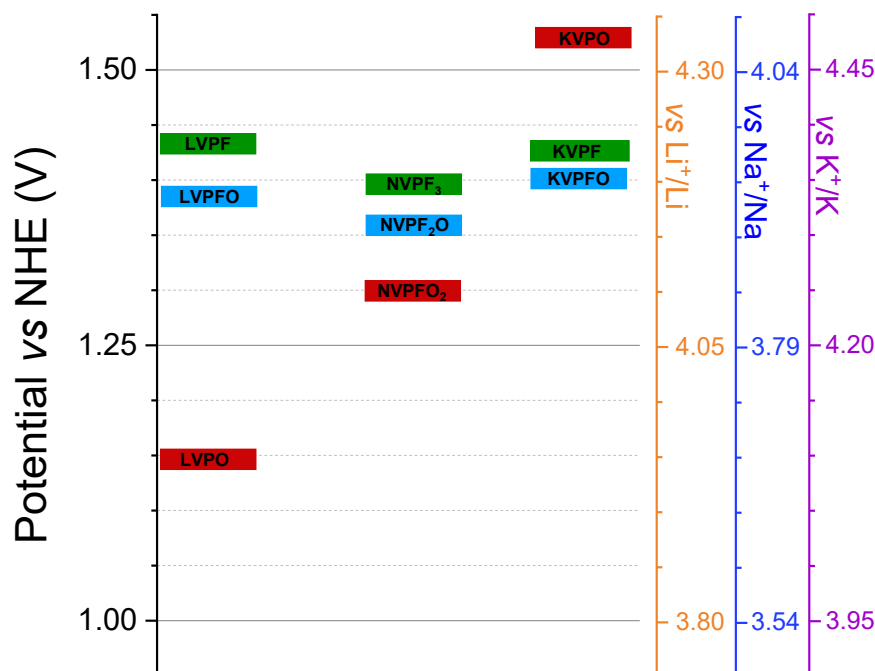


Figure 6: Average redox potential of the different $\text{LiVPO}_4(\text{F},\text{O})$, $\text{Na}_3\text{V}_2(\text{PO}_4)_2\text{F}(\text{F},\text{O})_2$ and $\text{KVPO}_4(\text{F},\text{O})$ compounds. Green rectangles correspond to vanadium fluoride phosphates, blue rectangles correspond to partially substituted compounds and red rectangles correspond to vanadyl phosphates. For KVPO_4 , the capacity limitation prevents the determination of the $\text{V}^{5+/4+}=\text{O}$ redox potential such that a slightly different method was used. The average redox potential was extrapolated from the trend observed in the $\text{K}_{1-0.5}\text{VOPO}_4$ composition domain compared to that of $\text{K}_{1-0.5}\text{VPO}_4\text{F}$.

CONCLUSIONS

Vanadium fluoride phosphates are promising electrode materials for high energy rechargeable alkali-ion batteries thanks to their high redox potentials and their capability to support long-term cycling. Alongside their potential application, they also exhibit a great diversity of crystal structures. Despite their closely related chemical formula ($\text{A}_{1+x}\text{VPO}_4\text{F}_{1+x}$ ($x = 0, 1/2$)), the structural framework depends strongly on the nature of the alkali ion and stoichiometry, as shown by the formation of Tavorite LiVPO_4F , Tavorite NaVPO_4F and $\text{Na}_3\text{V}_2(\text{PO}_4)_2\text{F}_3$, as well as KTP-type KVPO_4F . In these materials, fluoride anions can be partly or fully substituted, leading to the formation of vanadium oxyfluoride phosphates or oxide phosphates, respectively. Structural peculiarities lead to different behaviours at the local scale: the substituted oxygens tend to segregate in LiVPO_4F due to cooperative vanadyl distortions, but distribute randomly in $\text{Na}_3\text{V}_2(\text{PO}_4)_2\text{F}_3$ and KVPO_4F . The replacement of ionic $\text{V}^{3+}-\text{F}$ by highly covalent $\text{V}^{4+}=\text{O}$ bonds in the mixed O/F compounds results in significant changes in the physicochemical properties, redox mechanisms, and electrode potentials. During alkali ion de-insertion, end-member compounds undergo biphasic reactions due to alkali – vacancy orderings while partially substituted compounds tend to behave as solid solutions owing to anion disorder which breaks local periodicity. The redox potential of these compounds is affected by up to 350 mV difference between the F^- and O^{2-} compounds and up to 0.5 V compared to non-mixed anion phosphates such as $\text{Na}_3\text{V}_2(\text{PO}_4)_3$. Mixed

anion chemistry is therefore one of the most promising routes that can be used to tune the electrochemical behaviour of these polyanionic systems.

AUTHOR INFORMATION

Corresponding authors

Laurence Croguennec – Univ. Bordeaux, CNRS, Bordeaux INP, ICMCB, UMR 5026, F-33600 Pessac, France; RS2E, Réseau sur le Stockage Electrochimique de l’Energie, FR CNRS 3459, Amiens F-80039 Cedex 1, France; ALISTORE-ERI European Research Institute, FR CNRS 3104, F-80039 Amiens Cedex 1, France; orcid.org/0000-0002-3018-0992; Email: Laurence.Croguennec@icmcb.cnrs.fr

Romain Wernert – Univ. Bordeaux, CNRS, Bordeaux INP, ICMCB, UMR 5026, F-33600 Pessac, France; ICGM, Univ. Montpellier, CNRS, ENSCM, Montpellier, France; RS2E, Réseau sur le Stockage Electrochimique de l’Energie, FR CNRS 3459, Amiens F-80039 Cedex 1, France; orcid.org/0000-0002-5073-4008; Email: Romain.Wernert@chem.ox.ac.uk

Present address: Department of Chemistry, Inorganic Chemistry Laboratory, University of Oxford, Oxford OX1 3QR, UK

Authors

Dany Carlier – Univ. Bordeaux, CNRS, Bordeaux INP, ICMCB, UMR 5026, F-33600 Pessac, France; RS2E, Réseau sur le Stockage Electrochimique de l’Energie, FR CNRS 3459, Amiens F-80039 Cedex 1, France; ALISTORE-ERI European Research Institute, FR CNRS 3104, F-80039 Amiens Cedex 1, France; orcid.org/0000-0002-5086-4363

Long H.B. Nguyen – ICGM, Université de Montpellier, CNRS, ENSCM, 34095 Montpellier, France; RS2E, Réseau Français sur le Stockage Electrochimique de l’Energie, FR CNRS #3459, Amiens F-80039 Cedex 1, France; <https://orcid.org/0000-0001-7823-1595>

ACKNOWLEDGEMENTS

This work was part of the TROPIC project supported by Agence Nationale de la Recherche (ANR) under the grant ANR-19-CE05-0026. ANR is also acknowledged for funding the RS2E network through the STORE-EX Labex Project ANR-10-LABX-76-01, as well as Région Nouvelle Aquitaine for the support of these researches through the funding of synthesis and characterization equipment. LC and DC thank also Christian Masquelier and Jean-Noël Chotard from LRCS-UPJV (Amiens, France) and Edouard Boivin presently in IMMM (Le Mans, France) for their collaboration on crystallochemistry of polyanionic materials.

REFERENCES

- (1) Schindler, M.; Hawthorne, F. C.; Baur, W. H. Crystal Chemical Aspects of Vanadium: Polyhedral Geometries, Characteristic Bond Valences, and Polymerization of (VOn) Polyhedra. *Chem. Mater.* **2000**, *12* (5), 1248–1259. <https://doi.org/10.1021/cm990490y>.
- (2) Boudin, S.; Guesdon, A.; Leclaire, A.; Borel, M.-M. Review on Vanadium Phosphates with Mono and Divalent Metallic Cations: Syntheses, Structural Relationships and Classification, Properties. *International Journal of Inorganic Materials* **2000**, *2* (6), 561–579. [https://doi.org/10.1016/S1466-6049\(00\)00074-X](https://doi.org/10.1016/S1466-6049(00)00074-X).
- (3) Goodenough, J. B.; Hong, H. Y.-P.; Kafalas, J. A. Fast Na⁺-Ion Transport in Skeleton Structures. *Materials Research Bulletin* **1976**, *11* (2), 203–220. [https://doi.org/10.1016/0025-5408\(76\)90077-5](https://doi.org/10.1016/0025-5408(76)90077-5).
- (4) Delmas, C.; Olazcuaga, R.; Cherkaoui, F.; Brochu, R.; Le Flem, G. Sur Une Nouvelle Famille de Phosphates de Formule Na₃M₂(PO₄)₃ (M = Ti, V, Cr, Fe). *Comptes rendus hebdomadaires des séances de l'Académie des sciences. Série C, Sciences chimiques* **1978**, *287*, 169–171.
- (5) Barker, J.; Saidi, M. Y.; Swoyer, J. L. Electrochemical Insertion Properties of the Novel Lithium Vanadium Fluorophosphate, LiVPO₄F. *ChemInform* **2004**, *35* (3). <https://doi.org/10.1002/chin.200403013>.
- (6) Barker, J.; Saidi, M. Y.; Swoyer, J. L. Electrochemical Properties of Beta-LiVOPO₄ Prepared by Carbothermal Reduction. *Journal of The Electrochemical Society*.
- (7) Le Meins, J.-M.; Crosnier-Lopez, M.-P.; Hemon-Ribaud, A.; Courbion, G. Phase Transitions in the Na₃M₂(PO₄)₂F₃ Family (M=Al³⁺, V³⁺, Cr³⁺, Fe³⁺, Ga³⁺): Synthesis, Thermal, Structural, and Magnetic Studies. *Journal of Solid State Chemistry* **1999**, *148* (2), 260–277. <https://doi.org/10.1006/jssc.1999.8447>.
- (8) Fedotov, S. S.; Khasanova, N. R.; Samarin, A. Sh.; Drozhzhin, O. A.; Batuk, D.; Karakulina, O. M.; Hadermann, J.; Abakumov, A. M.; Antipov, E. V. AVPO₄F (A = Li, K): A 4 V Cathode Material for High-Power Rechargeable Batteries. *Chem. Mater.* **2016**, *28* (2), 411–415. <https://doi.org/10.1021/acs.chemmater.5b04065>.
- (9) Benhamada, L.; Grandin, A.; Borel, M. M.; Leclaire, A.; Raveau, B. KVPO₅, an Intersecting Tunnel Structure Closely Related to the Hexagonal Tungsten Bronze. *Acta Crystallographica Section C* **1991**, *47* (6), 1138–1141. <https://doi.org/10.1107/S0108270190014044>.
- (10) Hasa, I.; Mariyappan, S.; Saurel, D.; Adelhelm, P.; Kuposov, A. Y.; Masquelier, C.; Croguennec, L.; Casas-Cabanas, M. Challenges of Today for Na-Based Batteries of the Future: From Materials to Cell Metrics. *Journal of Power Sources* **2021**, *482*, 228872. <https://doi.org/10.1016/j.jpowsour.2020.228872>.
- (11) Boivin, E.; David, R.; Chotard, J.-N.; Bamine, T.; Iadecola, A.; Bourgeois, L.; Suard, E.; Fauth, F.; Carlier, D.; Masquelier, C.; Croguennec, L. LiVPO₄F₁–YO_y Favorite-Type Compositions: Influence of the Concentration of Vanadyl-Type Defects on the Structure and Electrochemical Performance. *Chem. Mater.* **2018**, *30* (16), 5682–5693. <https://doi.org/10.1021/acs.chemmater.8b02138>.
- (12) Nguyen, L. H. B.; Broux, T.; Camacho, P. S.; Denux, D.; Bourgeois, L.; Belin, S.; Iadecola, A.; Fauth, F.; Carlier, D.; Olchowka, J.; Masquelier, C.; Croguennec, L. Stability in Water and Electrochemical Properties of the Na₃V₂(PO₄)₂F₃ – Na₃(VO)₂(PO₄)₂F Solid Solution. *Energy Storage Materials* **2019**, *20*, 324–334. <https://doi.org/10.1016/j.ensm.2019.04.010>.
- (13) Wernert, R.; Nguyen, L. H. B.; Petit, E.; Camacho, P. S.; Iadecola, A.; Longo, A.; Fauth, F.; Stievano, L.; Monconduit, L.; Carlier, D.; Croguennec, L. Controlling the Cathodic Potential of KVPO₄F through Oxygen Substitution. *Chem. Mater.* **2022**, *34* (10), 4523–4535. <https://doi.org/10.1021/acs.chemmater.2c00295>.
- (14) Boivin, E.; Chotard, J.-N.; Bamine, T.; Carlier, D.; Serras, P.; Palomares, V.; Rojo, T.; Iadecola, A.; Dupont, L.; Bourgeois, L.; Fauth, F.; Masquelier, C.; Croguennec, L. Vanadyl-Type Defects in Favorite-like NaVPO₄F: From the Average Long Range Structure to Local Environments. *J. Mater. Chem. A* **2017**, *5* (47), 25044–25055. <https://doi.org/10.1039/C7TA08733K>.
- (15) Chen, S.; Wu, C.; Shen, L.; Zhu, C.; Huang, Y.; Xi, K.; Maier, J.; Yu, Y. Challenges and Perspectives for NASICON-Type Electrode Materials for Advanced Sodium-Ion Batteries. *Advanced Materials* **2017**, *29* (48), 1700431. <https://doi.org/10.1002/adma.201700431>.
- (16) Nguyen, L. H. B.; Chen, F.; Masquelier, C.; Croguennec, L. Polyanionic-Type Compounds as Positive Electrodes for Na-Ion Batteries. In *Na-ion Batteries*; John Wiley & Sons, Ltd, 2021; pp 47–100. <https://doi.org/10.1002/9781119818069.ch2>.

- (17) Ni, Q.; Bai, Y.; Wu, F.; Wu, C. Polyanion-Type Electrode Materials for Sodium-Ion Batteries. *Advanced Science* **2017**, *4* (3), 1600275. <https://doi.org/10.1002/advs.201600275>.
- (18) Bianchini, M.; Brisset, N.; Fauth, F.; Weill, F.; Elkaim, E.; Suard, E.; Masquelier, C.; Croguennec, L. Na₃V₂(PO₄)₂F₃ Revisited: A High-Resolution Diffraction Study. *Chem. Mater.* **2014**, *26* (14), 4238–4247. <https://doi.org/10.1021/cm501644g>.
- (19) Nguyen, L. H. B.; Iadecola, A.; Belin, S.; Olchowka, J.; Masquelier, C.; Carlier, D.; Croguennec, L. A Combined Operando Synchrotron X-Ray Absorption Spectroscopy and First-Principles Density Functional Theory Study to Unravel the Vanadium Redox Paradox in the Na₃V₂(PO₄)₂F₃–Na₃V₂(PO₄)₂FO₂ Compositions. *J. Phys. Chem. C* **2020**, *124* (43), 23511–23522. <https://doi.org/10.1021/acs.jpcc.0c06967>.
- (20) Boivin, É. Crystal Chemistry of Vanadium Phosphates as Positive Electrode Materials for Li-Ion and Na-Ion Batteries. Doctoral dissertation, Université de Picardie - Jules Verne, Amiens, 2017.
- (21) Bamine, T.; Boivin, E.; Masquelier, C.; Croguennec, L.; Salager, E.; Carlier, D. Local Atomic and Electronic Structure in the LiVPO₄(F,O) Tavorite-Type Materials from Solid-State NMR Combined with DFT Calculations. *Magnetic Resonance in Chemistry* **2020**, *58* (11), 1109–1117. <https://doi.org/10.1002/mrc.5059>.
- (22) Fedotov, S. S.; Luchinin, N. D.; Aksyonov, D. A.; Morozov, A. V.; Ryazantsev, S. V.; Gaboardi, M.; Plaisier, J. R.; Stevenson, K. J.; Abakumov, A. M.; Antipov, E. V. Titanium-Based Potassium-Ion Battery Positive Electrode with Extraordinarily High Redox Potential. *Nat Commun* **2020**, *11* (1), 1484. <https://doi.org/10.1038/s41467-020-15244-6>.
- (23) Kim, H.; Seo, D.-H.; Bianchini, M.; Clément, R. J.; Kim, H.; Kim, J. C.; Tian, Y.; Shi, T.; Yoon, W.-S.; Ceder, G. A New Strategy for High-Voltage Cathodes for K-Ion Batteries: Stoichiometric KVPO₄F. *Advanced Energy Materials* **2018**, *8* (26), 1801591. <https://doi.org/10.1002/aenm.201801591>.
- (24) Park, Y.-U.; Seo, D.-H.; Kim, H.; Kim, J.; Lee, S.; Kim, B.; Kang, K. A Family of High-Performance Cathode Materials for Na-Ion Batteries, Na₃(VO_{1-x}PO₄)₂F_{1+2x} (0 ≤ x ≤ 1): Combined First-Principles and Experimental Study. *Adv. Funct. Mater.* **2014**, *24* (29), 4603–4614. <https://doi.org/10.1002/adfm.201400561>.
- (25) Park, Y.-U.; Seo, D.-H.; Kwon, H.-S.; Kim, B.; Kim, J.; Kim, H.; Kim, I.; Yoo, H.-I.; Kang, K. A New High-Energy Cathode for a Na-Ion Battery with Ultrahigh Stability. *J. Am. Chem. Soc.* **2013**, *135* (37), 13870–13878. <https://doi.org/10.1021/ja406016j>.
- (26) Hardcastle, F. D.; Wachs, I. E. Determination of Vanadium-Oxygen Bond Distances and Bond Orders by Raman Spectroscopy. *J. Phys. Chem.* **1991**, *95* (13), 5031–5041. <https://doi.org/10.1021/j100166a025>.
- (27) Olchowka, J.; Fang, R.; Nuernberg, R. B.; Pablos, C.; Carlier, D.; Cassaignon, S.; Croguennec, L. Particle Nanosizing and Coating with an Ionic Liquid: Two Routes to Improve the Transport Properties of Na₃V₂(PO₄)₂FO₂. *Nanoscale* **2022**, *14* (24), 8663–8676. <https://doi.org/10.1039/D2NR01080A>.
- (28) Nguyen, L. H. B.; Sanz Camacho, P.; Broux, T.; Olchowka, J.; Masquelier, C.; Croguennec, L.; Carlier, D. Density Functional Theory-Assisted ³¹P and ²³Na Magic-Angle Spinning Nuclear Magnetic Resonance Study of the Na₃V₂(PO₄)₂F₃–Na₃V₂(PO₄)₂FO₂ Solid Solution: Unraveling Its Local and Electronic Structures. *Chem. Mater.* **2019**, *31* (23), 9759–9768. <https://doi.org/10.1021/acs.chemmater.9b03546>.
- (29) Li, C.; Shen, M.; Lou, X.; Hu, B. Unraveling the Redox Couples of VIII/VIV Mixed-Valent Na₃V₂(PO₄)₂O_{1.6}F_{1.4} Cathode by Parallel-Mode EPR and In Situ/Ex Situ NMR. *J. Phys. Chem. C* **2018**, *122* (48), 27224–27232. <https://doi.org/10.1021/acs.jpcc.8b09151>.
- (30) Serras, P.; Palomares, V.; Alonso, J.; Sharma, N.; López Del Amo, J. M.; Kubiak, P.; Fdez-Gubieda, M. L.; Rojo, T. Electrochemical Na Extraction/Insertion of Na₃V₂O_{2x}(PO₄)₂F_{3-2x}. *Chem. Mater.* **2013**, *25* (24), 4917–4925. <https://doi.org/10.1021/cm403679b>.
- (31) Liu, Z.; Hu, Y.-Y.; Dunstan, M. T.; Huo, H.; Hao, X.; Zou, H.; Zhong, G.; Yang, Y.; Grey, C. P. Local Structure and Dynamics in the Na Ion Battery Positive Electrode Material Na₃V₂(PO₄)₂F₃. *Chem. Mater.* **2014**, *26* (8), 2513–2521. <https://doi.org/10.1021/cm403728w>.
- (32) Messenger, R. J.; Ménétrier, M.; Salager, E.; Boulineau, A.; Duttine, M.; Carlier, D.; Ateba Mba, J.-M.; Croguennec, L.; Masquelier, C.; Massiot, D.; Deschamps, M. Revealing Defects in Crystalline Lithium-Ion Battery Electrodes by Solid-State NMR: Applications to LiVPO₄F. *Chem. Mater.* **2015**, *27* (15), 5212–5221. <https://doi.org/10.1021/acs.chemmater.5b01234>.
- (33) Bamine, T.; Boivin, E.; Boucher, F.; Messenger, R. J.; Salager, E.; Deschamps, M.; Masquelier, C.; Croguennec, L.; Ménétrier, M.; Carlier, D. Understanding Local Defects in Li-Ion Battery Electrodes

- through Combined DFT/NMR Studies: Application to LiVPO₄F. *J. Phys. Chem. C* **2017**, *121* (6), 3219–3227. <https://doi.org/10.1021/acs.jpcc.6b11747>.
- (34) Shraer, S. D.; Luchinin, N. D.; Trussov, I. A.; Aksonov, D. A.; Morozov, A. V.; Ryazantsev, S. V.; Iarchuk, A. R.; Morozova, P. A.; Nikitina, V. A.; Stevenson, K. J.; Antipov, E. V.; Abakumov, A. M.; Fedotov, S. S. Development of Vanadium-Based Polyanion Positive Electrode Active Materials for High-Voltage Sodium-Based Batteries. *Nat Commun* **2022**, *13* (1), 4097. <https://doi.org/10.1038/s41467-022-31768-5>.
- (35) Mba, J.-M. A.; Croguennec, L.; Basir, N. I.; Barker, J.; Masquelier, C. Lithium Insertion or Extraction from/into Tavorite-Type LiVPO₄F: An In Situ X-Ray Diffraction Study. *J. Electrochem. Soc.* **2012**, *159* (8), A1171–A1175. <https://doi.org/10.1149/2.022208jes>.
- (36) Dacek, S. T.; Richards, W. D.; Kitchaev, D. A.; Ceder, G. Structure and Dynamics of Fluorophosphate Na-Ion Battery Cathodes. *Chem. Mater.* **2016**, *28* (15), 5450–5460. <https://doi.org/10.1021/acs.chemmater.6b01989>.
- (37) Wernert, R.; Nguyen, L. H. B.; Iadecola, A.; Weill, F.; Fauth, F.; Monconduit, L.; Carlier, D.; Croguennec, L. Self-Discharge Mechanism of High-Voltage KVPO₄F for K-Ion Batteries. *ACS Appl. Energy Mater.* **2022**, *5* (12), 14913–14921. <https://doi.org/10.1021/acsaem.2c02379>.
- (38) Wernert, R.; Iadecola, A.; Stievano, L.; Carlier, D.; Croguennec, L. Origin of Vanadium Site Sequential Oxidation in K_xVPO₄F_{1–y}O_y. *Chem. Mater.* **2023**, *35* (2), 617–627. <https://doi.org/10.1021/acs.chemmater.2c03132>.
- (39) Liu, Y.; Rong, X.; Bai, R.; Xiao, R.; Xu, C.; Zhang, C.; Xu, J.; Yin, W.; Zhang, Q.; Liang, X.; Lu, Y.; Zhao, J.; Chen, L.; Hu, Y.-S. Identifying the Intrinsic Anti-Site Defect in Manganese-Rich NASICON-Type Cathodes. *Nat Energy* **2023**, 1–9. <https://doi.org/10.1038/s41560-023-01301-z>.
- (40) Park, S.; Chotard, J.-N.; Carlier, D.; Moog, I.; Courty, M.; Duttine, M.; Fauth, F.; Iadecola, A.; Croguennec, L.; Masquelier, C. Crystal Structures and Local Environments of NASICON-Type Na₃FeV(PO₄)₃ and Na₄FeV(PO₄)₃ Positive Electrode Materials for Na-Ion Batteries. *Chem. Mater.* **2021**, *33* (13), 5355–5367. <https://doi.org/10.1021/acs.chemmater.1c01457>.
- (41) Park, S.; Chotard, J.-N.; Carlier, D.; Fauth, F.; Iadecola, A.; Masquelier, C.; Croguennec, L. Irreversible Electrochemical Reaction at High Voltage Induced by Distortion of Mn and V Structural Environments in Na₄MnV(PO₄)₃. *Chem. Mater.* **2023**, *35* (8), 3181–3195. <https://doi.org/10.1021/acs.chemmater.2c03787>.
- (42) Chen, F.; Kovrugin, V. M.; David, R.; Mentré, O.; Fauth, F.; Chotard, J.-N.; Masquelier, C. A NASICON-Type Positive Electrode for Na Batteries with High Energy Density: Na₄MnV(PO₄)₃. *Small Methods* **2019**, *3* (4), 1800218. <https://doi.org/10.1002/smt.201800218>.
- (43) Zhou, W.; Xue, L.; Lü, X.; Gao, H.; Li, Y.; Xin, S.; Fu, G.; Cui, Z.; Zhu, Y.; Goodenough, J. B. Na_xMV(PO₄)₃ (M = Mn, Fe, Ni) Structure and Properties for Sodium Extraction. *Nano Lett.* **2016**, *16* (12), 7836–7841. <https://doi.org/10.1021/acs.nanolett.6b04044>.

TABLE OF CONTENT FIGURE

